

---

# Finite Element Analysis of Solar Sail Force Model with Mission Application

Proc IMechE Part G:  
J Aerospace Engineering  
2019, Vol. 233(5):1838–1846  
©IMechE 2018  
Article reuse guidelines:  
sagepub.com/journals-permissions  
DOI:10.1177/0954410018764183  
journals.sagepub.com/home/pig

Luisa Boni, Giovanni Mengali and Alessandro A. Quarta\*

*Department of Civil and Industrial Engineering, University of Pisa, I-56122 Pisa, Italy*

## Abstract

A finite element approach is used to calculate the components of forces and moments acting on a square solar sail at a Sun-sail distance equal to one astronomical unit. The model takes into account the deformation effect induced by the solar radiation pressure, where the incidence of the reflected photons changes as a function of the local orientation of the sail surface. Assuming a specular reflection model, the analysis shows that the maximum value of the transversal thrust component takes place when the solar zenith angle is about 36 deg, which is in accordance with the result available for a classical flat solar sail. Notably, the modulus of the moment due to the solar radiation pressure takes its maximum value approximately at the same (solar zenith) angle.

## Keywords

Square solar sail, solar sail force model, Finite Element Analysis, sail mission, near-optimal control law

## Nomenclature

$a_c$	=	maximum propulsive acceleration at $r = 1$ au, [mm/s <sup>2</sup> ]
$\mathbf{F}$	=	resultant force (with $F \triangleq \ \mathbf{F}\ $ ), [N]
$J_M, J_F$	=	dimensionless performance index
$k_M, k_F$	=	dimensionless parameter
$\mathbf{M}$	=	resultant moment (with $M \triangleq \ \mathbf{M}\ $ ), [N]
$O$	=	origin of $\mathcal{T}$ , nominal center of the sail
$\mathbf{r}$	=	sail-Sun vector (with $r \triangleq \ \mathbf{r}\ $ ), [au]
$T$	=	orbital period, [days]
$\mathcal{T}(O; x, y, z)$	=	body reference frame
$\alpha$	=	solar zenith angle, [deg]
$\phi$	=	solar azimuth angle, [deg]
$\Delta t$	=	flight time, [days]

---

\* Corresponding author; e-mail: a.quarta@ing.unipi.it

*Subscripts*

$i$	=	initial
$f$	=	final
max	=	maximum
opt	=	optimal
$r$	=	radial
$t$	=	transversal

*Superscripts*

$\star$	=	maximum of $F_t$
$\wedge$	=	unit vector

**1. Introduction**

A fundamental requirement during the planning of a space mission is the availability of an accurate mathematical model for the description of the spacecraft thrust vector characteristics. This is a particularly important issue when the spacecraft is propelled by a solar sail. In fact, in that case the thrust vector characteristics are closely related to the sail's shape, to its billowing effect due to the solar radiation pressure, and to the thermo-optical characteristics of the reflecting film <sup>1,2</sup>.

Different models for the description of the solar sail thrust vector are available in the literature <sup>3</sup>. The simplest model, referred to as ideal model, assumes the solar sail surface to be flat and specularly reflecting. A refined version of this model, called optical force model <sup>4</sup>, takes into account the thermo-optical characteristics of the reflecting film, although the previous assumption of flat shape is maintained. The optical force model is still sufficiently simple from an analytical viewpoint and actually represents the reference model for most study of solar sail-based space missions <sup>5</sup>, even when the degradation effect of the sail reflecting film is considered <sup>6,7</sup>. When the sail billowing effect due to the solar radiation pressure is accounted for, the study of the thrust vector becomes a difficult problem to solve even under the simplification of specular reflection of the sail surface. In that case, the best known is the parametric force model, which derives from a numerical analysis of the actual sail deformation performed at JPL at the end of the 1970s, during a preliminary study of a rendezvous mission toward Halley's comet <sup>3,4</sup>. The strength of the parametric model is in its capability of relating in a simple and direct way the thrust vector direction with the sail attitude orientation through an interpolation of numerical-experimental data. Its weakness is that its results cannot be easily applied to sail configurations different from those used during the interpolation process.

A generalized model <sup>8,9</sup> is sometimes used to describe the thrust of a solar sail with a nonplanar surface, having arbitrary and non-deformable shape. This model, which has also been used to analyze the performance of axially symmetric solar sails <sup>10</sup>, is however unsuitable for describing the billowing effect caused by the solar radiation pressure. A possible solution to this problem is to calculate the thrust vector characteristics, as a function of the sail attitude, by means of a Finite Element (FE) analysis <sup>11,12</sup>. An interesting and thorough discussion of the available literature about this method applied to solar sails can be found in the review paper by Fu et al. <sup>5</sup>. Other studies about a square sail configuration, with special attention to the interaction between the sail shape and the thrust characteristics, are available in Refs. [13,14,15,16,17,18,19].

In this context, the authors <sup>20</sup> have recently proposed a technique for the deformation analysis of a square solar sail under realistic loading conditions, with the aid of the commercial software ABAQUS V 6.11 <sup>21</sup>.

In particular, the model of Ref. [20] is representative of the whole square sail structure, and has been used to investigate the sail structural response in presence of pre-tensioning, surface, and inertial loads, while the external loads are balanced in accordance with the inertia relief principle <sup>22</sup>.

The developed FE analysis takes into account the geometrical non-linear behavior of the model by means of an implicit non-linear analysis, based on a Newton-Raphson algorithm, without the need of any non-zero stabilization parameter. The non-linear analysis is performed on an initial geometrical configuration perturbed with a linear combination of the first four global buckling modes, obtained with a previous eigenvalue analysis. In this context, a multi-step approach has been used: in the first step the sail membranes have been pre-stressed, then, in the second step, a uniform surface load, which simulates the force induced by the solar radiation pressure, has been applied to the pre-stressed sail surface. In the multi-step analysis, each next step starts in the stress/strain conditions calculated at the end of the previous step. Due to the strongly non-linear behavior of the sail membrane, a preliminary sail pre-tensioning is necessary to obtain the numerical convergence when the solar pressure is applied. In the second step, the inertia relief method, an advanced option implemented within software ABAQUS V 6.11 <sup>21</sup>, has been used to simulate the “free flight” condition of the spacecraft. Such a method allows unconstrained structures to be simulated with a static analysis, using the inertia of the structure to resist the applied loadings. In particular, a rigid body acceleration is applied to the structure, consistent with its actual mass distribution, which produces inertial forces that balance the external applied forces. Accordingly, the assumption is made that the structure is in a state of static equilibrium even though it is not constrained.

The aim of this paper is to use the model discussed in Ref. [20] to calculate, as a function of the spacecraft attitude, the components of forces and moments acting on a solar sail placed at a Sun-sail distance equal to one astronomical unit (this situation is representative of a sail deployment just outside the Earth’s sphere of influence). In particular, the FE analysis <sup>20</sup> is used to predict the loads acting on a 20 m × 20 m square solar sail for different values of the angle of incidence of the solar radiation, where the incident and the reflected photons are taken into account with separate contributions.

## 2. Model description and numerical results

Consider a square solar sail configuration and introduce a body reference frame  $\mathcal{T}(O; x, y, z)$  whose origin is at the sail center, see Fig. 1. According to McInnes <sup>3</sup>, the plane  $(x, y)$  coincides with the nominal plane of the sail reflecting film, the  $x$ -axis is along one solar sail boom, while the  $z$ -axis is orthogonal to the sail illuminated surface, in the direction opposite to the thrust. The solar zenith angle  $\alpha \in [0, \pi/2]$  and solar azimuth angle  $\phi \in [0, 2\pi]$  are used to univocally define the unit position vector  $\hat{\mathbf{r}}$ , directed from the spacecraft to the Sun’s center-of-mass, see Fig. 1. In this case, the solar azimuth angle  $\phi$  is measured counterclockwise from the  $x$ -axis, whereas the solar zenith angle  $\alpha$  is the angle between the direction of  $\hat{\mathbf{r}}$  and the  $z$ -axis. Note that the solar zenith angle coincides with the more common sail cone angle <sup>3</sup>, defined as the angle between the normal to the (nominal) sail surface in the direction opposite to the Sun, and the solar radiation direction. In particular, the cone angle (i.e. the solar zenith angle in Fig. 1) is, together with the clock angle <sup>3</sup>, one of the two classical control parameters in a solar sail-based trajectory.

When a flat sail model is assumed, that is, when the deformation induced by the external loads is neglected, the angle of incidence of the photons is the same for each portion of the reflecting surface and is equal to  $\alpha$ , since the direction of the local normal to the surface is constant, see Fig. 1. The situation changes when the sail billowing effect due to the solar radiation pressure is taken into account. In fact, in that case each point of the reflective film experiences a different angle of incidence of the solar radiation, which depends on the local sail deformation, that is, on the direction of the local normal to the sail surface.

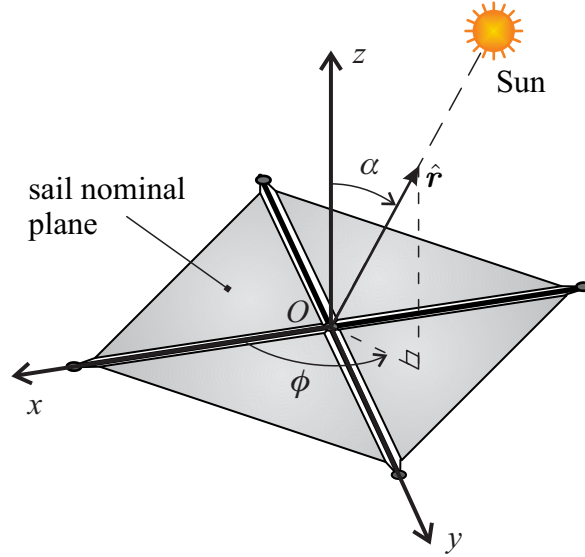


**Figure 1.** Reference frame and angles  $\alpha$  (solar zenith) and  $\phi$  (solar azimuth) of the spacecraft-Sun unit vector  $\hat{r}$ .

To model this behavior, in the development of the FE model the direction of the force acting on the sail surface due to the incident photons has been kept constant, while the direction of the load coming from the reflected photons has been changed during the analysis, in accordance with the local orientation of the normal to the elementary sail surface. In this context, a script in Python language has been developed to automatically launch the analyses and extract the results for a given range of values of the two solar angles  $\{\alpha, \phi\}$ , see Fig. 2. Such a methodology can be easily extended to the case of a reflective film with an optical force model, by enforcing a direction for the reflected rays that depends on the local optical properties of the sail surface. In that case, the incidence of the reflected rays should follow the rotation of the local normal, in such a way that the resultant force is not aligned with the normal to the surface, but tilts by an angle depending on the local optical properties of the sail film (recall that, in a perfectly reflecting film, the contribution of the reflected rays is such that the resultant is directed along the local normal to the sail elementary surface).

A square solar sail with a total mass of 72 kg and a side length of 20 m has been assumed in the analysis, whose material properties<sup>18,23,24</sup> are taken from Ref. [20]. Two different sail configurations, with either five or multiple connected points between the sail membranes and the reinforcing booms<sup>20</sup> have been analyzed, see Fig. 3. However, for the sake of space, only the results involving the sail with multiple connected points will now be discussed. In fact, the results relevant to the five points configurations are qualitatively very similar to those here presented. The only difference between the two configurations is introduced by the slightly different structure flexibility: the out-of-plane deflection is larger for the 5 points configurations, since each sail sector is globally less constrained to be deflected. For a sail with a side of 20 m, the effects on the resultant forces and moments are practically negligible.

In particular, the mesh model for the sail membranes is dominated by 4-node doubly curved shell S4 elements<sup>21</sup>, which are able to capture the slightest bending stress that can affect the sail during the loading phases and to deal with sail areas in compression and subjected to possible wrinkling phenomena. An example of mesh, as well as the main components of the sail structure, are shown in Figs. 3(c)-3(d). The supporting booms and the control mast are modeled with B31 beam elements, while the cables with T3D2 truss elements. Point masses have been used for the concentrated masses, located at the four tips of the booms, at the free end of the control mast and at the center of the spacecraft. A structured meshing technique has been used for each part of the FE

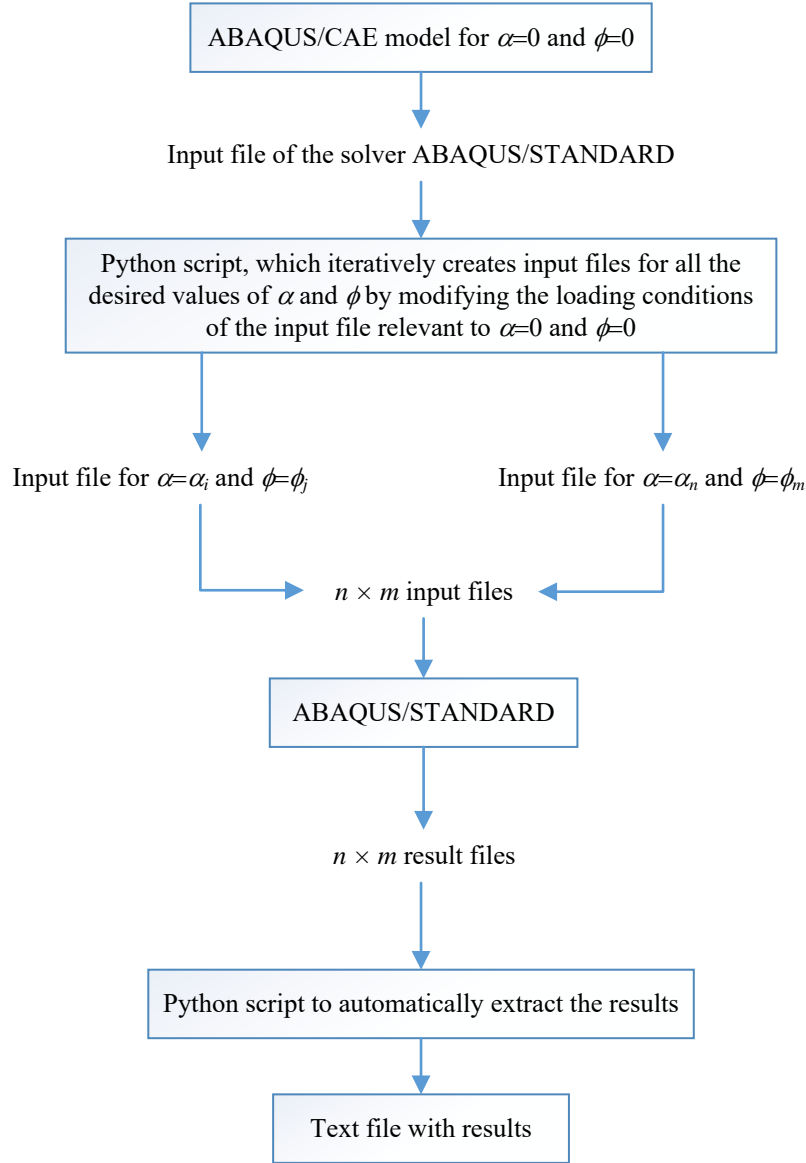


**Figure 2.** Numerical procedure for the calculation of forces and moments.

models. In particular, the model with multiple attachment points has been derived from the model with five connections by adding inner cables equally spaced along the booms.

The cables have been connected to the boom and to the sail sectors by means of connectors with a section of basic translational type (joint). The pre-tensioning of the cables has been realized by means of a predefined initial field of stress, applied to the truss elements. The pre-tensioning load has been selected such that the stress in the central part of each sail sector is about 1 Psi, a value sufficient to avoid the presence of large region in compression and, consequently, the occurrence of detrimental wrinkling. The pre-tensioning forces have action-lines convergent to the sail center, and their magnitude is the smallest possible to obtain a numerical convergence in the second step. Different directions of the forces generate a non-uniform pre-stress field in the sail. According to Ref. [20], pre-stress fields lower than 1 Psi at the sail center inhibit the convergence, while the occurrence

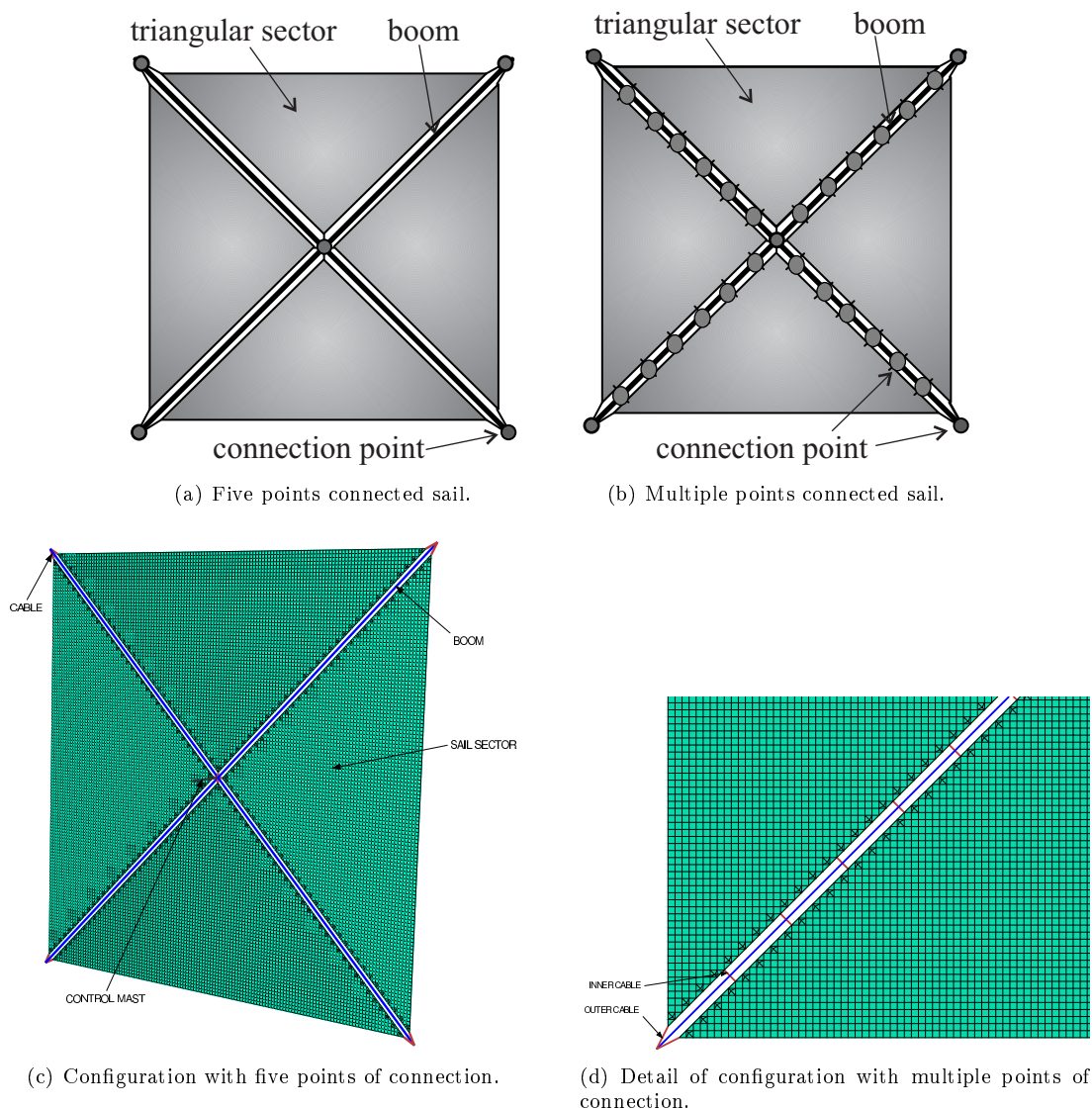


**Figure 3.** Square solar sail models (taken from Ref. [20]).

of wrinkles at the sail edges is promoted when the pre-stress exceeds about 1 Psi. Finally, the distribution of residual compressed regions after pre-tensioning is estimated in Ref. [20].

The (dimensionless) components of the resultant force  $\mathbf{F}$  and moment  $\mathbf{M}$  acting on the solar sail are shown in Fig. 4 as a function of the solar angles  $\alpha$  and  $\phi$ . The results have been obtained using software ABAQUS V 6.11<sup>21</sup> with the procedure discussed in Ref. [20] and assuming a perfectly reflecting sail film. In fact, a specular reflection model guarantees a simple validation of the numerical data with the results available from the literature. A more refined reflection model has not been considered in the analysis, as it would have required a full definition of the thermo-optical characteristics of the reflecting film, with a consequent addition of other parameters to be included within the validation process of the numerical results. In principle, however, the numerical approach<sup>20</sup> allows the actual properties of the reflecting film to be easily introduced in the analysis.

The results of the FE analyses have confirmed, for the considered square  $20\text{ m} \times 20\text{ m}$  solar sail, a fundamental symmetry of the resultant forces and moments. As a matter of fact, starting from a perfectly symmetrical

geometry of the spacecraft, an asymmetry of the resultant forces and moments can be induced by a non-negligible asymmetrical pattern of the strain field. Such a kind of asymmetry, if the thermal loads are neglected and the sail size is relatively small, is mainly due to modelling problems. Indeed, the lack of refinement and regularity of the mesh induces differences in the orientation of the local normal to the sail element, which results in an unsymmetrical deformation. The use of a structured, very fine and regular mesh made of S4 elements avoids the occurrence of this kind of problem.

For those reasons, the results refer to a single sail sector (which implies that the variation range of the solar azimuth angle is  $\phi \in [0, \pi/2]$ ) and are shown in Fig. 4, where  $F_{\max} \simeq 3.648 \text{ mN}$  (or  $M_{\max} \simeq 2.67 \mu\text{Nm}$ ) is the maximum modulus of the resultant force (or resultant moment) due to the solar radiation pressure at a Sun-spacecraft distance of one astronomical unit. The maximum sail propulsive acceleration at 1 au is equal to  $0.0507 \text{ mm/s}^2$ , a value typical for a low-performance solar sail. For comparative purposes, the Japanese square solar sail demonstrator IKAROS<sup>25</sup> provides a maximum propulsive acceleration of about  $0.0045 \text{ mm/s}^2$ , with a side length of 14 m and a spacecraft mass of 307 kg (including a sail mass of about 16 kg). As expected, Fig. 4 shows that the resultant force  $\mathbf{F}$  is nearly directed along the  $z$ -axis and is independent of the solar azimuth angle, while the resultant moment  $\mathbf{M}$  is approximately belonging to the sail nominal plane ( $x, y$ ). The presence of force components in the sail plane ( $F_x$  and  $F_y$ ) and a moment  $M_z$  orthogonal to the sail plane is due to the sail billowing induced by the solar radiation pressure. The difference in the order of magnitude of  $F_x$  and  $F_y$  compared to  $F_z$  as well as that of  $M_z$  compared to  $M_x$  and  $M_y$  varies, of course, with the sail side length. A more useful representation of the thrust vector is given in Fig. 5(a), where the radial ( $F_r$ ) and transversal ( $F_t$ ) components of the resultant force  $\mathbf{F}$  are shown in dimensionless form as a function of the solar zenith angle. In particular,  $F_r$  (or  $F_t$ ) is the component of  $\mathbf{F}$  along (perpendicular to) the direction of the sail-Sun unit vector  $\hat{\mathbf{r}}$ . Note that the signs of  $F_r$  and  $F_z$  are both negative since the  $z$ -axis is perpendicular to the illuminated sail surface<sup>3</sup>. From Fig. 1, the components of the sail-Sun unit vector  $\hat{\mathbf{r}}$ , in the body reference frame  $\mathcal{T}(O; x, y, z)$ , are

$$[\hat{\mathbf{r}}]_{\mathcal{T}} = \begin{bmatrix} \sin \alpha \cos \phi \\ \sin \alpha \sin \phi \\ \cos \alpha \end{bmatrix} \quad (1)$$

Therefore,  $F_r$  and  $F_t$  can be written as a function of  $\alpha$  and  $\phi$  as

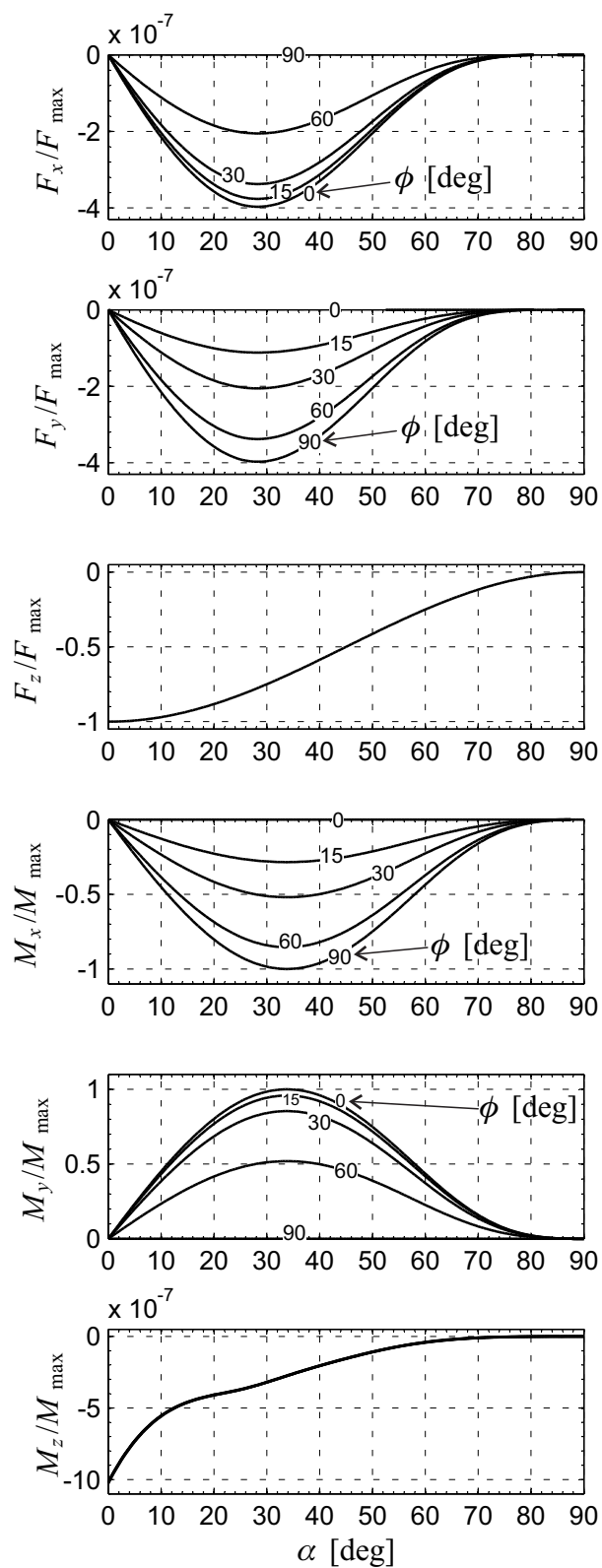
$$F_r = \mathbf{F} \cdot \hat{\mathbf{r}} = F_x \sin \alpha \cos \phi + F_y \sin \alpha \sin \phi + F_z \cos \alpha \quad (2)$$

$$F_t = \|\mathbf{F} - F_r \hat{\mathbf{r}}\| \quad (3)$$

Figure 5(a) shows that the maximum value of the transversal component  $F_t$  is reached at a solar zenith angle of about  $\alpha^* \triangleq 36 \text{ deg}$ . This is in agreement with the well known result<sup>3</sup> according to which the maximum value of the transversal thrust component for an ideal (perfectly reflecting) sail is obtained when the cone angle is  $\arcsin(1/\sqrt{3}) \text{ rad} \simeq 35.2 \text{ deg}$ .

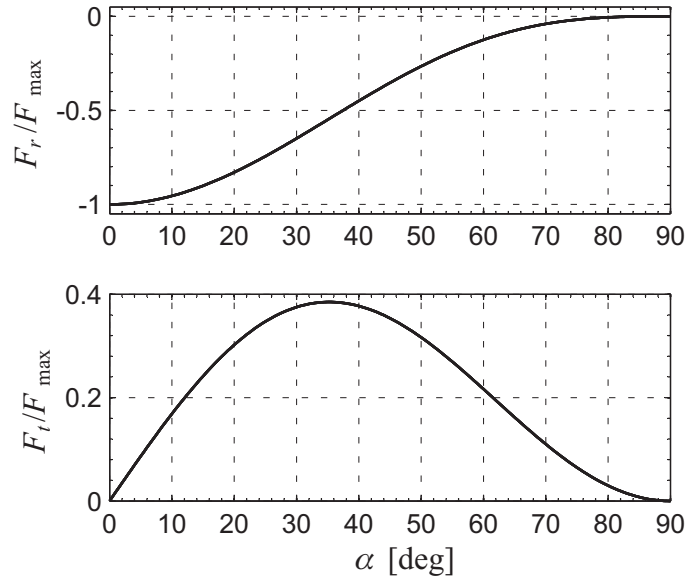
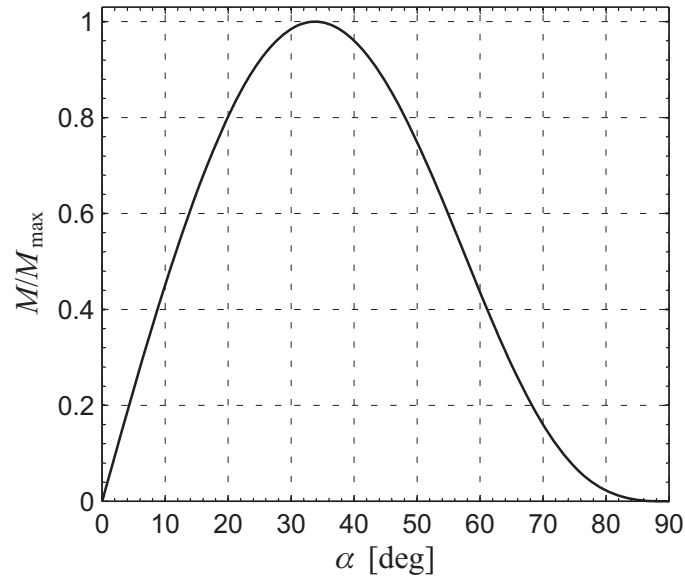
### 2.1. Tradeoff analysis

The FE analysis shows that the modulus  $M = \|\mathbf{M}\|$  of the resultant moment due to the solar radiation pressure is nearly independent of the solar azimuth angle  $\phi$  and its maximum value takes place at a solar zenith angle close to  $\alpha^*$ , see Fig. 5(b). This is a noteworthy result, since the solar zenith angle that maximizes  $F_t$  (that is,  $\alpha^*$ ) is of great importance in the study of optimal trajectories of solar sail-based spacecraft. For example, the maximum value of  $F_t$  is required in a near-optimal heliocentric orbit raising (or lowering) from a circular parking orbit<sup>26,27</sup>. Moreover, the FE numerical analysis confirms that  $M$  is close to its maximum when  $F_t$  is



**Figure 4.** Components of the force  $F$  and moment  $M$  due to the solar radiation pressure.



(a) Radial ( $F_r$ ) and transversal ( $F_t$ ) force.

(b) Moment modulus.

**Figure 5.** Dimensionless solar sail force and moment as a function of the solar zenith angle.

maximum, that is, the optimal transversal thrust and the optimal sail control authority are nearly obtained for the same spacecraft attitude. Indeed, most solar sail attitude control systems operate by shifting the center of mass with respect to the center of light pressure (or vice versa), as is discussed in the textbook of Vulpetti et al.<sup>28</sup>. In particular, they lose their control authority when the cone angle (or the solar zenith angle) approaches 90deg, that is, when both the total thrust and the moment modulus go to zero.

However, the fact that the modulus of  $F_z$  is about 70% of  $F_{\max}$  when  $F_t$  is maximum may represent a possible problem to be accounted for in the development phase of the control law. In fact, according to Vulpetti et al.<sup>28</sup>, unbalanced (or, in general, disturbance) moments arise when the center-of-pressure is shifted from its nominal position by an unwanted (and difficult to measure) distance. In this case, considering a pitch-axis dynamical

model of the solar sail and taking into account the comprehensive analysis of Wie<sup>29,30</sup>, the disturbance moment modulus is proportional to the component of  $\mathbf{F}$  along the direction perpendicular to the sail nominal plane, i.e. proportional to  $|F_z|$ .

Since high values of transversal thrust (or high control authority) are associated to medium-high values of  $|F_z|$ , it is useful to consider a tradeoff analysis involving the maximization of a suitable scalar performance index, defined as

$$J_F(\alpha, k_F) \triangleq (1 - k_F) \frac{F_t}{F_{t_{\max}}} - k_F \frac{|F_z|}{F_{z_{\max}}} \quad (4)$$

for the transversal thrust, and

$$J_M(\alpha, k_M) \triangleq (1 - k_M) \frac{M}{M_{\max}} - k_M \frac{|F_z|}{F_{z_{\max}}} \quad (5)$$

for the control authority, where  $F_{t_{\max}}$  is the maximum value of  $F_t$ , and  $F_{z_{\max}}$  is the maximum value of  $|F_z|$ . The rationale is that  $J_F$  (or  $J_M$ ) regulates the relative importance of  $F_t$  (or  $M$ ) and  $|F_z|$  through the dimensionless weight  $k_F \in [0, 1]$  (or  $k_M \in [0, 1]$ ), where a small value of  $k_F$  (or  $k_M$ ) implies that  $F_t$  (or  $M$ ) is the dominant term of  $J_F$  (or  $J_M$ ). In fact,  $k_F = 0$  (or  $k_M = 0$ ) corresponds to the limiting case  $J_F \equiv F_t/F_{\max}$  (or  $J_M \equiv M/M_{\max}$ ) and, as such,  $J_F$  (or  $J_M$ ) is maximum when the solar zenith angle is equal to (or about)  $\alpha^*$ . If instead  $k_F = 1$  or  $k_M = 1$ ,  $J_F \equiv J_M = -|F_z|/F_{z_{\max}}$  and the maximum value of the performance index is obtained when the modulus of  $F_z$  is zero, that is, when the solar zenith angle is  $\alpha = 90$  deg and the solar sail loses both its control authority and its propulsive acceleration.

For an intermediate value of  $k_F$  (or  $k_M$ ), the maximization of  $J_F$  (or  $J_M$ ) is obtained when the solar zenith angle is

$$\alpha_{\text{opt}_i}(k_i) = \max_{\alpha \in [0, \pi/2]} J_i(\alpha, k_i) \quad \text{with} \quad i = \{F, M\} \quad (6)$$

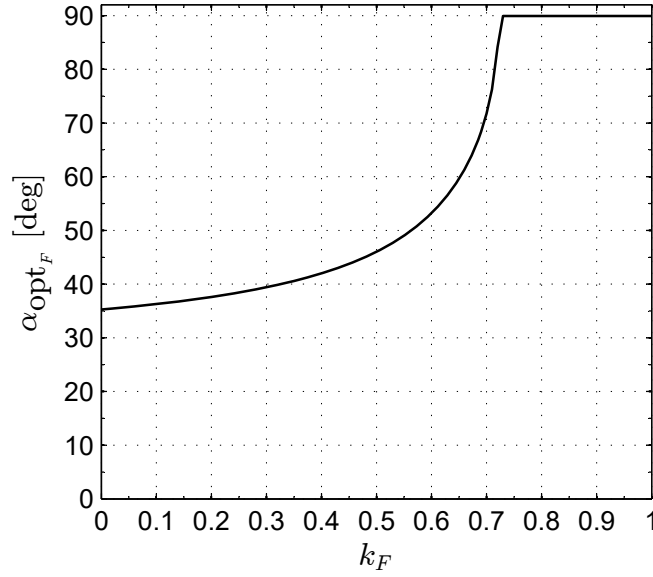
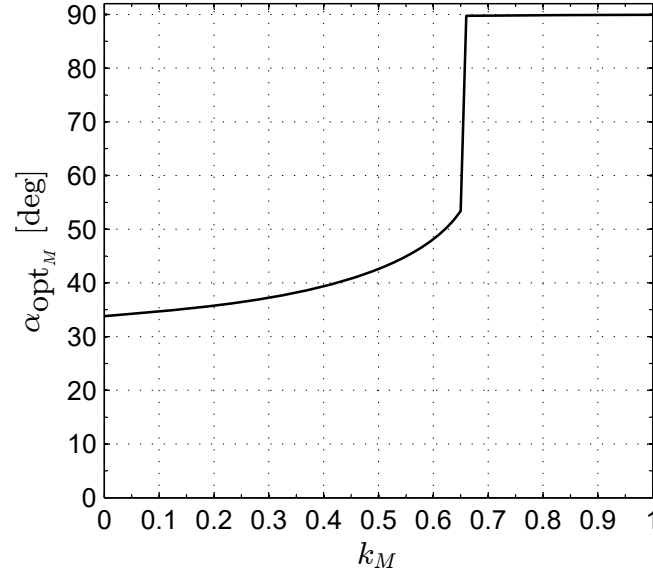
The solution of the optimum problem (6) has been obtained with a numerical approach based on the Nelder-Mead simplex method<sup>31</sup>, and is drawn in Fig. 6. The fact that  $\alpha_{\text{opt}_i} = 90$  deg for sufficiently large values of  $k_i$  is related to the particular topology of the isocontour lines of the function  $J_i = J_i(\alpha, k_i)$ . In fact, as is shown in Fig. 7, beyond a certain value of  $k_i$ ,  $J_i$  is an increasing function of  $\alpha$  and, therefore, takes its maximum when the solar zenith angle is maximum.

### 3. Mission application

The function  $\alpha_{\text{opt}_i}(k_i)$  may be effectively used in the preliminary phase of mission design. For illustrative purposes, a solar sail is assumed to be initially placed along a heliocentric circular orbit with radius  $r_0 = 1$  au. Consider a circle-to-circle orbit lowering, with the aim of reaching a final circular orbit of radius  $r_f = 0.99$  au. This scenario is representative, for example, of a transfer mission toward the collinear Sun-Earth Lagrangian point  $L_1$ , which is placed along the Sun-Earth line at a distance of about 0.01 au from our planet.

Paralleling the procedure discussed in Ref. [27], in which the cone angle (i.e. the solar zenith angle) is held constant during the orbital transfer, it may be shown that, assuming a perfectly reflecting low-performance solar sail, the minimum transfer time  $\Delta t$  is given by

$$\frac{\Delta t}{T_0} = \frac{a_{\oplus}}{6 \pi a_c} \left| \sqrt{r_f^3/r_0^3} - 1 \right| \quad (7)$$

(a) Conditions for a maximum of  $J_F$ .(b) Conditions for a maximum of  $J_M$ .**Figure 6.** Optimum solar zenith angle as a function of the dimensionless parameter  $k_F$  and  $k_M$ , see Eqs. (4)–(6).

where  $a_{\oplus} \triangleq 5.93 \text{ mm/s}^2$  is the modulus of the solar gravitational acceleration at 1 au,  $T_0 = 1 \text{ year}$  is the orbital period of the sail parking orbit (of radius  $r_0$ ), whereas  $a_c = 0.0507 \text{ mm/s}^2$  is the solar sail maximum propulsive acceleration at 1 au.

Bearing in mind the function  $F_t = F_t(\alpha)$  shown in Fig. 5(a), and recalling that the optimal solar zenith angle  $\alpha_{\text{opt}_F}$  (which maximizes  $J_F$ ) depends on  $k_F$  as is illustrated in Fig. 6(a), Eq. (7) provides a relation between the minimum flight time  $\Delta t$  and  $k_F$ , see Fig. 8. In particular, as long as  $k_F \leq 0.5$  the minimum flight time is nearly constant, since in this variation range of  $k_F$  the solar zenith angle is close to the value that maximizes  $F_t$  (about 36 deg), see Fig. 6. However, a marked increase of the flight time happens when  $k_F > 0.5$ , to such an extent that it doubles when  $k_F = 0.65$ , see Fig. 8. Note that the flight time  $\Delta t$  tends to infinity when  $k_F$  tends

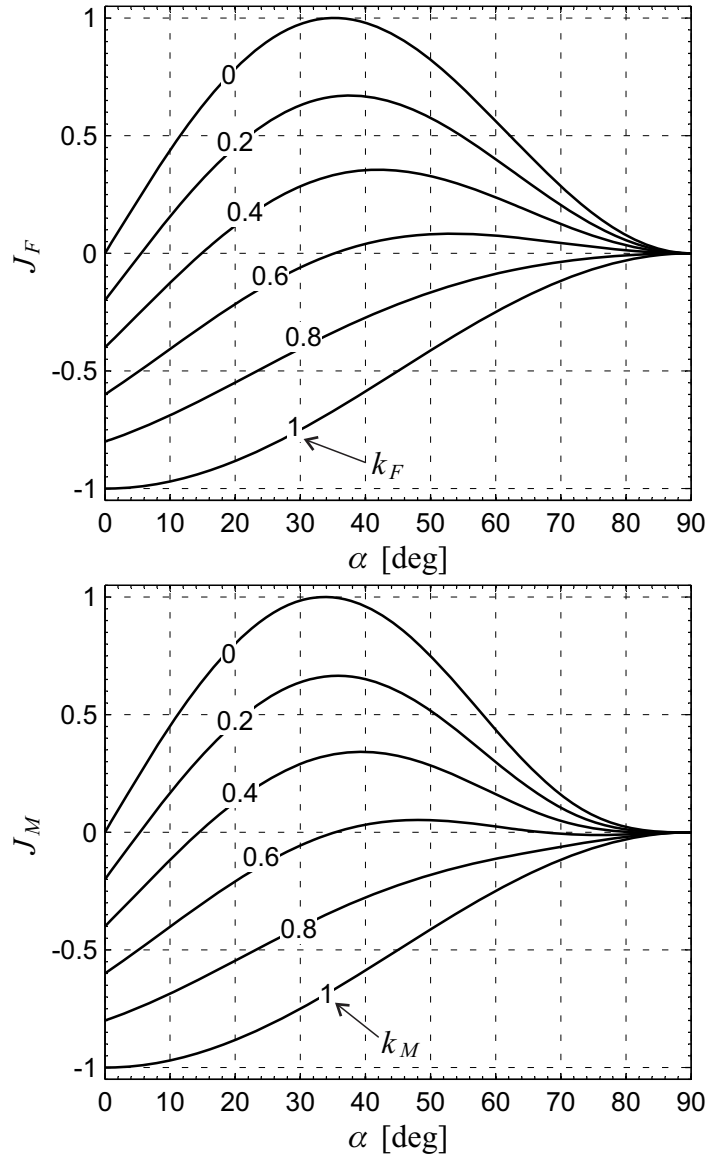


**Figure 7.** Level curves of the performance index  $J_i = J_i(\alpha, k_i)$ , with  $i = \{F, M\}$ , see Eqs. (4)-(5).

to 1 since, in this case,  $\alpha_{\text{opt}_F} \rightarrow 90$  deg and, therefore, the transversal thrust component  $F_t$  tends to zero, see Fig. 5(a).

#### 4. Conclusions

The main characteristics of the solar sail thrust vector have been obtained by means of a finite element analysis using the commercial software ABAQUS. The proposed procedure requires a reduced computational effort, and is able to provide an accurate description of the propulsive force (and total moment) as a function of the sail attitude. In particular, the maximum value of the moment modulus is reached at a solar zenith angle close to the angle that maximizes the transversal component of the thrust.

The natural extension of this work is to include the optical characteristics of the reflecting film in the study of both the thrust and the moment vector. In this context, the thermal analysis of the structure should also be

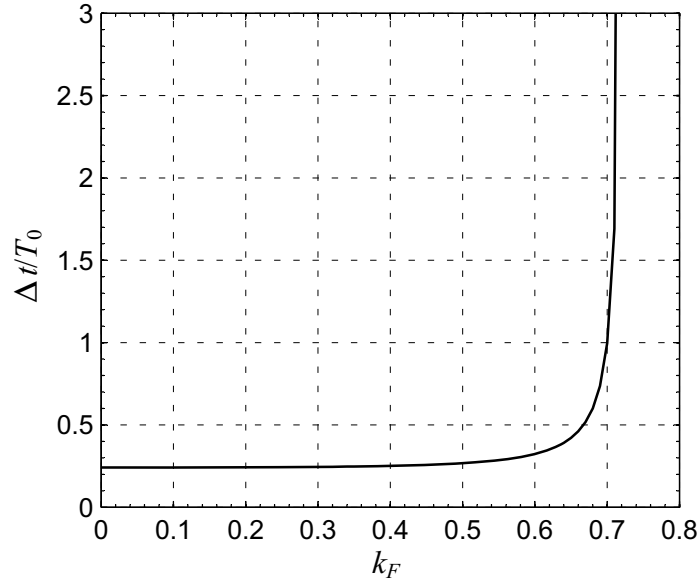


**Figure 8.** Dimensionless flight time  $\Delta t$  for a circle-to-circle optimal transfer ( $r_0 = 1$  au and  $r_f = 0.99$  au) as a function of  $k_F$ .

taken into account since, in principle, the thermal loads could have a non negligible effect on the sail deformation and so on the characteristics of the thrust-moment vector.

### Declaration of conflicting interests

The authors declared no potential conflicts of interest with respect to the research, authorship, and publication of this article.

### Funding

The authors received no financial support for the research, authorship, and publication of this article.

### References

- [1] Simo J, McInnes CR. Potential Effects of a Realistic Solar Sail and Comparison to an Ideal Sail. In: 26th AAS/AIAA Space Flight Mechanics Meeting; 2016. p. 3106–3120.
- [2] Ono G, Tsuda Y, Akatsuka K, et al. Generalized Attitude Model for Momentum-Biased Solar Sail Spacecraft. *Journal of Guidance, Control, and Dynamics*. 2016 July;39(7):1491–1500.
- [3] McInnes CR. In: *Solar Sailing: Technology, Dynamics and Mission Applications*. Springer-Praxis Series in Space Science and Technology. Berlin: Springer-Verlag; 1999. p. 46–53, 76–81.
- [4] Wright JL. In: Gordon, Breach, editors. *Space Sailing*. Gordon and Breach Science Publishers; 1992. p. 223–233.
- [5] Fu B, Sperber E, Eke F. Solar sail technology—A state of the art review. *Progress in Aerospace Sciences*. 2016 October;86:1–19.
- [6] Dachwald B, Mengali G, Quarta AA, et al. Parametric model and optimal control of solar sails with optical degradation. *Journal of Guidance, Control, and Dynamics*. 2006 September-October;29(5):1170–1178.
- [7] Dachwald B, Macdonald M, McInnes CR, et al. Impact of optical degradation on solar sail mission performance. *Journal of Spacecraft and Rockets*. 2007 July-August;44(4):740–749.

- [8] Rios-Reyes L, Scheeres DJ. Generalized Model for Solar Sails. *Journal of Spacecraft and Rockets*. 2005 January-February;42(1):182–185.
- [9] Rios-Reyes L, Scheeres DJ. Solar-Sail Navigation: Estimation of Force, Moments, and Optical Parameters. *Journal of Guidance, Control, and Dynamics*. 2007 May-June;30(3):660–668.
- [10] Mengali G, Quarta AA. Optimal control laws for axially symmetric solar sails. *Journal of Spacecraft and Rockets*. 2005 November-December;42(6):1130–1133.
- [11] Ewing A. Solar Sail Propulsion Sensitivity to Membrane Shape and Optical Properties Using the Solar Vectoring Evaluation Tool (SVET). In: 53rd Joint Army Navy Nasa Air Force (JANNAF) Propulsion Meeting. Monterey, CA; 2005.
- [12] Sakamoto H, Miyazaki Y, Park KC. Finite Element Modeling of Sail Deformation Under Solar Radiation Pressure. *Journal of Spacecraft and Rockets*. 2007 May-June;44(3):514–521.
- [13] Campbell BA, Thomas SJ. Realistic solar sail thrust. In: Macdonald M, editor. *Advances in Solar Sailing*. Springer Praxis Books. Springer Berlin Heidelberg; 2014. p. 407–435.
- [14] Murphy D, Murphey T, Gierow P. Scalable Solar Sail Subsystem Design Considerations. In: 43rd AIAA/ASME/ASCE/AHS/ASC Structures, Structural Dynamics, and Materials Conference. Denver, CO; 2002. Paper AIAA-2002-1703.
- [15] Ingrassia T, Faccin V, Bolle A, et al. Solar sail elastic displacement effects on interplanetary trajectories. *Acta Astronautica*. 2013 February;82(2):263–272.
- [16] Canfield SL, Peddieson J, Garbe G. Similarity criteria and associated design procedures for scaling solar sail systems. *Journal of Spacecraft and Rockets*. 2011 January-February;48(1):218–221.
- [17] Peloni A, Barbera D, Laurenzi S, et al. Dynamic and Structural Performances of a New Sailcraft Concept for Interplanetary Missions. *The Scientific World Journal*. 2015;2015. Article ID 714371.
- [18] Sleight D, Muheim D. Parametric Studies of Square Solar Sails Using Finite Element Analysis. In: 45th AIAA/ASME/ASCE/AHS/ASC Structures, Structural Dynamics & Materials Conference. Palm Springs, California; 2004. Paper AIAA 2004-1509.
- [19] Greschik G, Mikulas MM. Design Study of a Square Solar Sail Architecture. *Journal of Spacecraft and Rockets*. 2002 September-October;39(5):653–661.
- [20] Boni L, Mengali G, Quarta AA. Solar Sail Structural Analysis via Improved Finite Element Modeling. *Proceedings of the Institution of Mechanical Engineers, Part G: Journal of Aerospace Engineering*. 2016;In press.
- [21] Anon. Abaqus 6.11 Analysis User's Manual - Volume II: Analysis; 2011.
- [22] Liao L. A Study of Inertia Relief Analysis. In: 52nd AIAA/ASME/ASCE/AHS/ASC Structures, Structural Dynamics and Materials Conference. Denver, Colorado; 2011. Paper AIAA 2011-2002.
- [23] Liu J, Cui N, Shen F, et al. Dynamics of highly-flexible solar sail subjected to various forces. *Acta Astronautica*. 2014;103:55–72.
- [24] Jenkins CHM, editor. *Gossamer Spacecraft: Membrane And Inflatable Structures Technology For Space Applications*. vol. 191 of *Progress in Astronautics and Aeronautics*. American Institute of Aeronautics and Astronautics; 2001. ISBN: 978-1-56347-403-3.
- [25] Yamaguchi T, Mimasu Y, Tsuda Y, et al. Solar Sail Acceleration Modeling and its Estimation for IKAROS Spacecraft. In: *The 21th Workshop on JAXA Astrodynamics and Flight Mechanics*. Sagami-hara (Japan); 2011.
- [26] Macdonald M, Dachwald B. Heliocentric Solar Sail Orbit Transfers with Locally Optimal Control Laws. *Journal of Spacecraft and Rockets*. 2007 January-February;44(1):273–276.
- [27] Quarta AA, Mengali G. Semi-Analytical Method for the Analysis of Solar Sail Heliocentric Orbit Raising. *Journal of Guidance, Control, and Dynamics*. 2012 January-February;35(1):330–335.

- 
- [28] Vulpetti G, Johnson L, Matloff GL. 11. In: *Solar Sails: A Novel Approach to Interplanetary Travel*. New York: Springer-Verlag; 2015. p. 122–125.
  - [29] Wie B. Solar Sail Attitude Control and Dynamics, Part 1. *Journal of Guidance, Control, and Dynamics*. 2004 July-August;27(4):526–535.
  - [30] Wie B. Solar Sail Attitude Control and Dynamics, Part 2. *Journal of Guidance, Control, and Dynamics*. 2004 July-August;27(4):536–544.
  - [31] Lagarias JC, Reeds JA, Wright MH, Wright PE. Convergence Properties of the Nelder-Mead Simplex Method in Low Dimensions. *SIAM Journal on Optimization*. 1998 October-December;9(1):112–147.